Supplementary Information for

"Direct imaging of interlayer-coupled symmetric and antisymmetric plasmon modes in graphene/hBN/graphene heterostructures"

Cheng Hu[1,2†], Aolin Deng[1,2†*], Peiyue Shen[1,2†], Xingdong Luo[1,2], Xianliang Zhou[1,2], Tongyao Wu[1,2], Xinyue Huang[1,2], Yulong Dong[1,2], Kenji Watanabe[3], Takashi Taniguchi[4], Guibai Xie[5], Xiaojun Li[5], Qi Liang[1,2], Zhiwen Shi[1,2*]

[1]Key Laboratory of Artificial Structures and Quantum Control (Ministry of Education), Shenyang National Laboratory for Materials Science, School of Physics and Astronomy, Shanghai Jiao Tong University, Shanghai, 200240, China.

[2]Collaborative Innovation Center of Advanced Microstructures, Nanjing, 210093, China.

[3]Research Center for Functional Materials, National Institute for Materials Science, 1-1 Namiki, Tsukuba 305-0044, Japan.

[4]International Center for Materials Nanoarchitectonics, National Institute for Materials Science, 1-1 Namiki, Tsukuba 305-0044, Japan.

[5]National Key Laboratory of Science and Technology on Space Science, China Academy of Space Technology (Xi'an), Xi'an, China.

† These authors contribute equally to this work.

* To whom correspondence should be addressed. Email: zwshi@sjtu.edu.cn, daolin@sjtu.edu.cn.

Section S1. Numerical simulation model

The in-plane and out-of-plane permittivity of hBN are 8.7 and 4.1, respectively, for light at $\lambda_p = 10.6\ \mu m$. The SiO_2 optical data is from the COMSOL material database. The conductivity of graphene in the simulation model takes on a Drude-like form $\sigma_g = \frac{ie^2 E_F}{\pi\hbar^2(\omega + \frac{i}{\tau})}$. The electron relaxation time is expressed as $\tau = \frac{\mu E_F}{ev_F^2}$, where $v_F = c/300$ is the Fermi velocity in graphene, E_F is the Fermi energy, μ = 100,000 cm^2 V^{-1} s^{-1} is the DC mobility of graphene. The excitation source in the simulation is an electric dipole setting on the top-layer graphene surface. All the mash sizes are optimized to get the convergent results and all the results are in frequency domain.

Section S2. The Fourier transform of the line profile in the individual top- and bottom-layer graphene

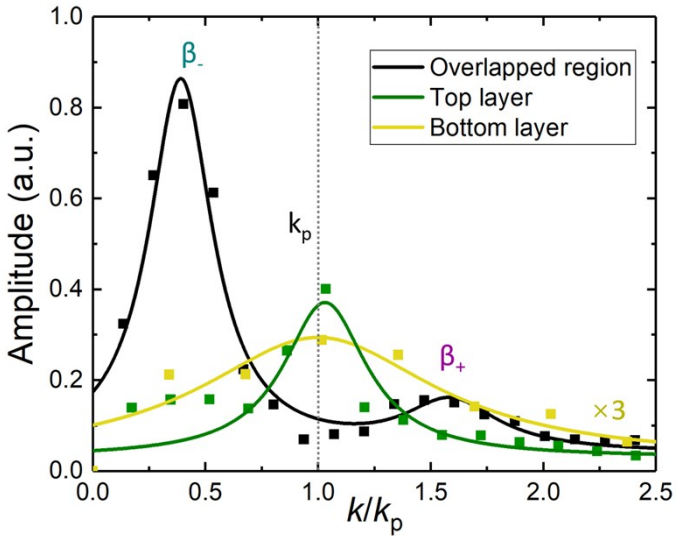

Fig. S1. The Fourier transform of the plasmon line profiles extracted from the top-layer graphene (green), bottom-layer graphene (yellow), and the overlapped coupling region (black) in Fig. 1d.

Section S3. Simulation results for the optimum coupling distance factor of the anti-symmetric mode detection

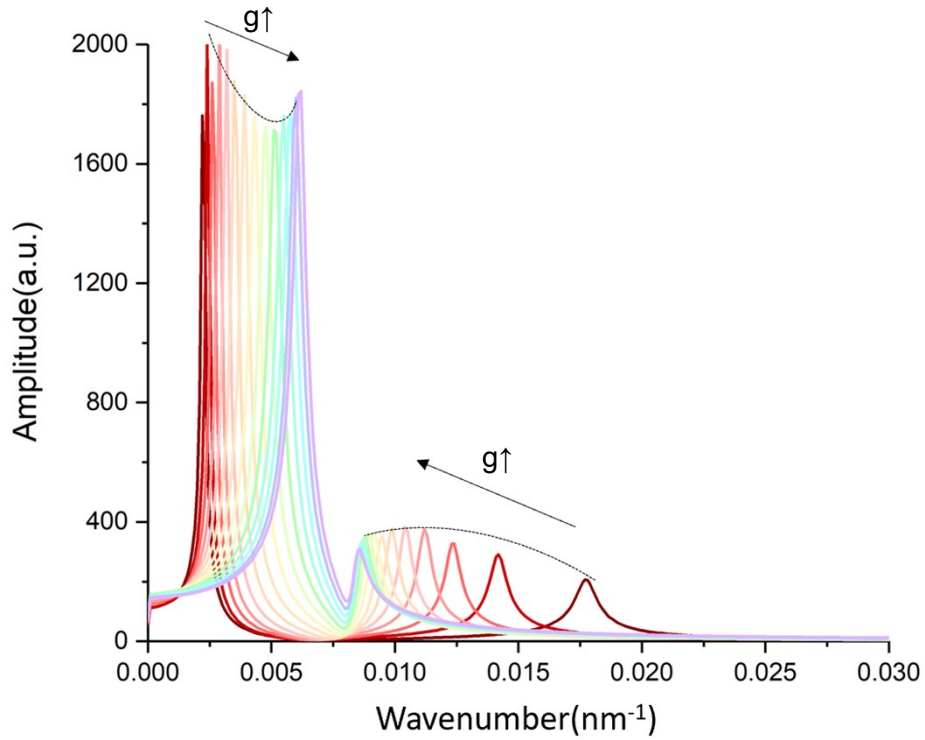

Fig. S2. The simulated evolution of the near-field amplitude distribution in the frequency domain with different coupling distance factors.

We set the electric field detectors at 10 nm away from the top-layer graphene to record the field distribution of the two coupling modes in different coupling factors g (g $= k_p \cdot d$). With the increased coupling factors g, the amplitude of the $\beta+$ mode increased in the beginning and decreased in the last, which indicate the existence of maximum amplitude indicates that there exists an optimum coupling distance factor g for the $\beta+$ mode detection. In the beginning, the coupling strength is strong, which cause the short wavelength of the $\beta+$ mode. Therefore, the electric field of $\beta+$ mode

decays fast and localizes near the graphene surface. When the coupling factors g increasing, the wavelength of $\beta+$ mode gets increasing. As a result, the amplitude increasing. On the other hand, the increasing of coupling factors g weakens the excite efficiency of $\beta+$ mode and therefore the amplitude of $\beta+$ mode decreased in the last.

Section S4. More evidences for the same intrinsic plasmon wavelength in overlapped and non-overlapped regions without plasmon-plasmon coupling

In our device 1, we have tuned back gate U_2 to investigate the plasmon wavelength change at the boundary of overlapped and non-overlapped regions, as shown in Fig. S3. The bottom-layer graphene is in charge neutral and displays no near-field response in this near field image when the back gate U_2 is tuned at -24 V with U_1 fixed at -5 V. It is obvious that the plasmon wavelength in overlapped and non-overlapped regions is continuous and almost the same when there doesn't exist coupling in graphene plasmons. Therefore, it is reasonable for us to use the plasmon wavelength in the non-overlapped region as uncoupled plasmon wavelength in the overlapped region.

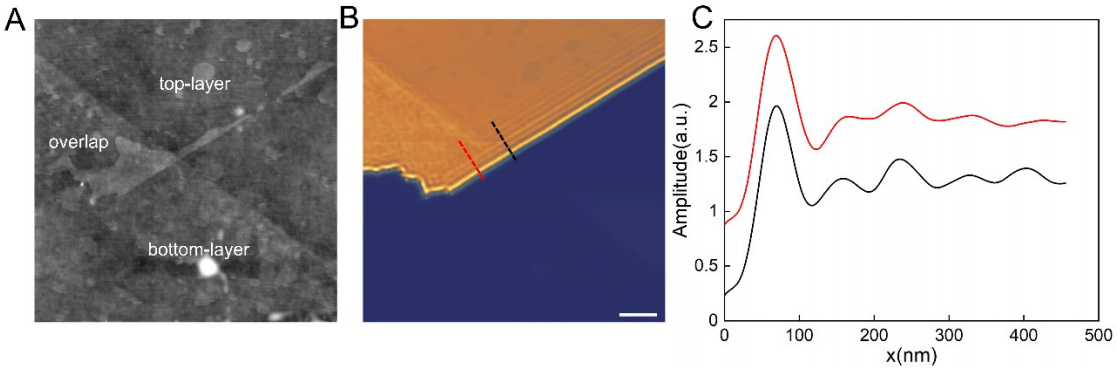

Fig. S3. A Topographic image of the device 1. **B** Near-field image when the bottom-layer graphene is in charge neutral. The gate U_1 and U_2 are -5 V and -24 V respectively. The scale bar are 0.5 um

in **A** and **B**. **C** Plasmon line profiles in **B**. The red curve is extracted in overlapped region and black curve is in non-overlapped region near the boundary.

We have also fabricated a sample with the hBN about 150 nm thick as shown in the inset of Fig. S4. The plasmon wavelength in overlapped region is about 138 nm with the gate U_1=40 V and U_2=0 V, which is shorter than the thickness of hBN layer (150 nm). The plasmon coupling between two layers can be neglected. We can see that the plasmon pattern are indeed consecutive and the wavelength are almost unchanged between the overlapped region and the non-overlapped region.

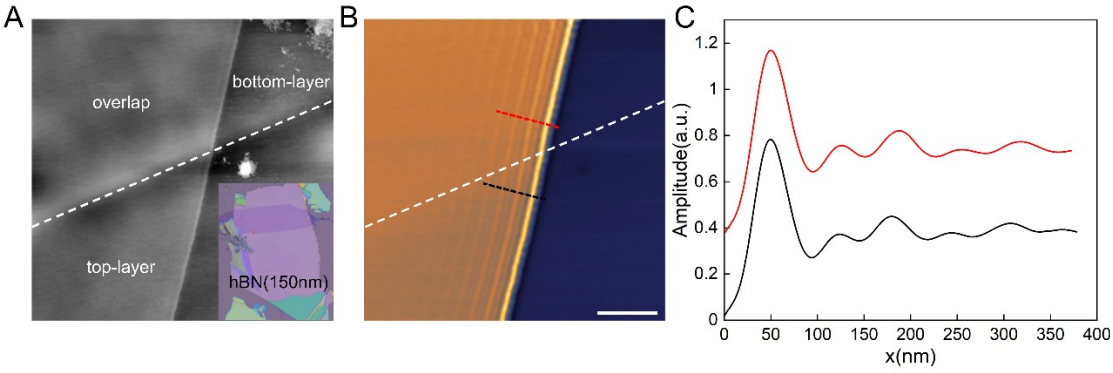

Fig. S4. A Topographic image of the sample. The inset is optical image with hBN about 150 nm. **B** Near-field image when the gate U_1=40 V, U_2=0 V. The plasmon is consecutive across the boundary with an almost unchanged wavelength. The scale bar in A and B are 0.5 um. **C** Plasmon line profiles in **B** with red curve extracted in overlapped region and black curve in non-overlapped region near the boundary.

Section S5. Quantum mechanical two energy levels coupling system

Firstly, we can assume a very simple coupling system, two level have the same energy E_0 without coupling. Therefore, we can write down its Hamiltonian as:

$$H=\begin{pmatrix} E_0 & 0 \\ 0 & E_0 \end{pmatrix} \tag{S1}$$

If we add a coupling energy κ into this system, which means that the off diagonal elements are not zero:

$$H=\begin{pmatrix} E_0 & \kappa \\ \kappa & E_0 \end{pmatrix} \tag{S2}$$

Then, we can get its eigenvalues $E=E_0 \pm \kappa$. Consider the dispersion of graphene plasmon:

$$k_p = \frac{\hbar^2\omega^2(1+\varepsilon_r)}{\pi e^2 E_F} \tag{S3}$$

In our experiment, the incident frequency ω is fixed. According to equation S3, we have:

$$\Delta k_p = \frac{2\hbar^2(1+\varepsilon_r)}{\pi e^2 E_F}\omega\,\Delta\omega \tag{S4}$$

Therefore, we can have this relation $\kappa = \hbar\Delta\omega$ if the coupling strength is weak enough. Here, we can get the dispersion relation of the coupling modes:

$$\beta_{\pm} = \frac{\hbar^2\omega^2(1+\varepsilon_r)}{\pi e^2 E_F} \pm \frac{2\hbar\omega(1+\varepsilon_r)}{\pi e^2 E_F}\kappa \tag{S5}$$

it is reasonable to assume that the coupling strength κ is proportional to $e^{-k_p d}$ because the electric field of each individual layer mode decays exponentially. Then we can get the evolution of coupling modes under different coupling distance factor g to fit into equation S5. Fig. S5 plot the evolution of the coupling modes. The gray lines are the fitting line using the formula S5. As the prediction, in the weak coupling region, the coupling behavior can be understood as a quantum mechanical two energy levels coupling.

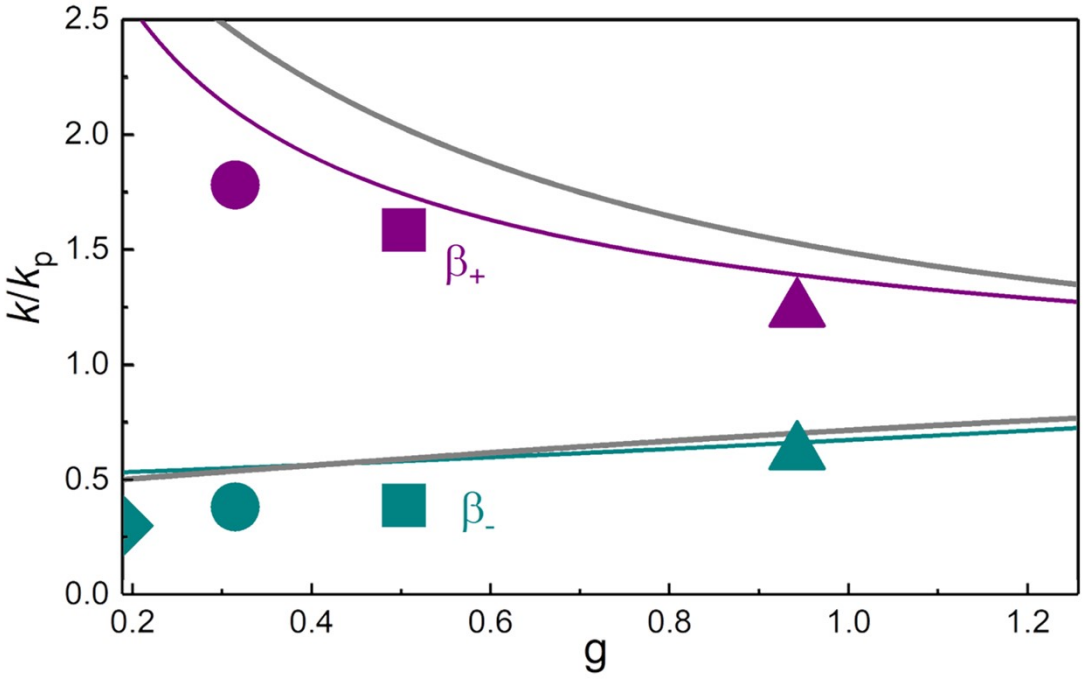

Fig. S5. Evolution of coupling modes with different coupling distance factor g. The two gray lines are the fitting lines using the formula S5.

Section S6. Q-factors of the coupling modes

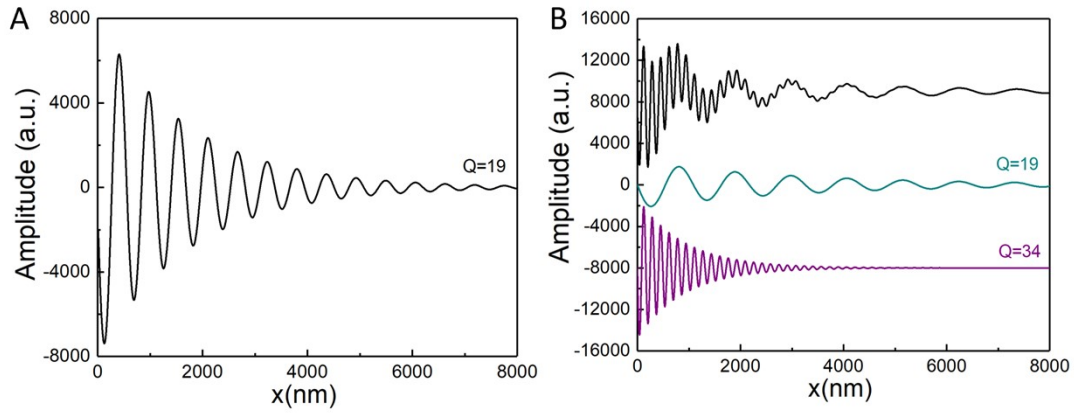

Fig. S6. A Simulation near-field line-profile of the monolayer graphene plasmons (Q=19) and **B** the two layers graphene coupling modes. The cyan and purple lines are the symmetric (Q=19) and anti-symmetric (Q=34) modes, respectively.

We calculate the near-field distribution of the monolayer graphene plasmon mode and the two layers graphene coupling modes, as shown in Fig. S6. To avoid the other loss channel, we set the graphene is around the vacuum environment. The graphene Fermi energy is 0.43 eV and the coupling factor g is 0.3. The simulation results show an interesting phenomenon that the coupling caused the mode split and reduce the electromagnetic loss of the anti-symmetric mode. It is worth to note that the Q-factor of the anti-symmetric mode (Q=34) can be higher than the intrinsic propagating mode (Q=19) on the monolayer graphene. It is due to the transverse electric field in the two layers graphene of the anti-symmetric mode is opposite, which caused weaker transverse electric field in the graphene layer and achieved the lower electromagnetic loss. It is indicated that the coupling phenomenon can reduce the intrinsic loss. Typically, there exist a trade-off between the Q-factor and the propagating wavelength. Such high Q-factor with high wavelength compression propagating mode is highly desired for the future novel low loss optical devices.

Section S7. Compare with the plasmon modes in a metal-insulator-metal (MIM) heterostructure and an insulator-metal-insulator (IMI) heterostructure

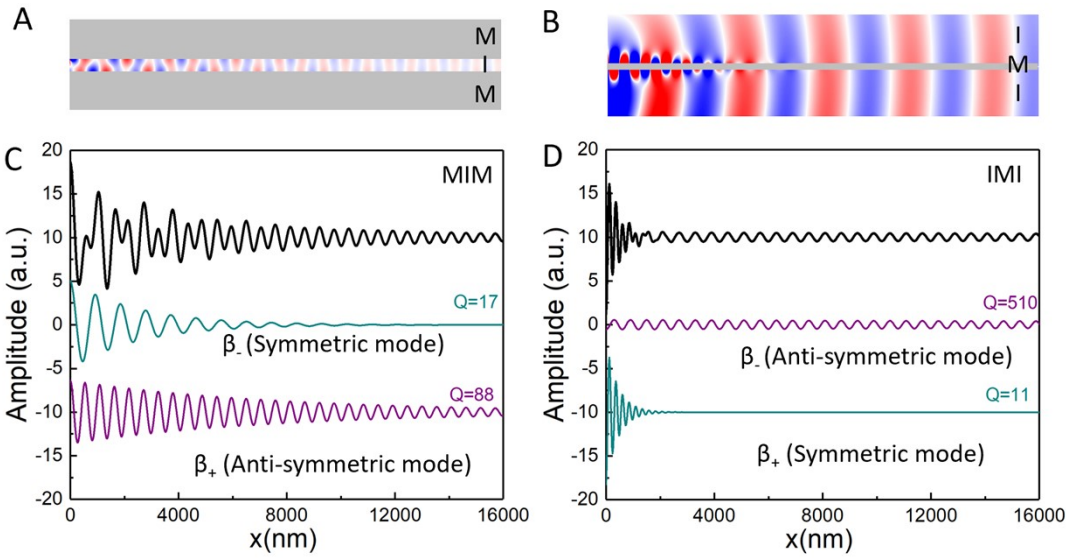

Fig. S7. A Simulation electric field (E_z) distribution of the MIM and **B.** IMI coupling modes, respectively. **C.** The electric field line-profile of the coupling modes of MIM and **D.** IMI. The cyan and purple lines are the symmetric and anti-symmetric modes, respectively.

We have simulated two types of traditional waveguides: the MIM waveguide and the IMI waveguide, as shown in Fig. S7. Our interlayer graphene plasmon coupling behavior is more like the MIM waveguide. The symmetric mode has longer wavelength and lower Q-factor compare with the anti-symmetric mode. It is the exact opposite for the IMI waveguide coupling modes. Its anti-symmetric mode has longer wavelength close to the free-space wavelength and have a higher Q-factor.